FAST AND ACCURATE COMPUTATION OF THE MINIMUM DISTANCE BETWEEN RSO TRAJECTORIES

Ana S. Rivero(1), Giulio Baù(2), Rafael Vazquez(1), Claudio Bombardelli(3)

(1) *Universidad de Sevilla, Escuela Técnica Superior de Ingeniería, Camino de los Descubrimientos s.n. 41092 Sevilla (Spain) , Email: {asanchez8, rvazquez1}@us.es*

(2) *Università di Pisa, Dipartimento di Matematica, Largo Bruno Pontecorvo, 5, 56127, Pisa (Italy) , Email: giulio.bau@unipi.it*

(3) *Universidad Politécnica de Madrid, Escuela Técnica Superior de Ingeniería Aeronáutica y del Espacio, Pza. del Cardenal Cisneros, 3, 28040, Madrid (Spain) , Email: claudio.bombardelli@upm.es*

ABSTRACT

The Minimum Orbit Intersection Distance (MOID), i.e. the smallest distance between two osculating orbits, is a key parameter in astrodynamics. Determining the MOID between Resident Space Objects (RSOs) is essential for conjunction assessment and space traffic management. Traditional Keplerian-based MOID approaches struggle to account for environmental perturbations that alter object trajectories over time, leading to reduced accuracy. This work presents a fast and accurate non-Keplerian MOID Assessment Tool (NKMAT) for estimating the minimum distance between non-coplanar RSOs in low Earth orbit with small eccentricities, encompassing the majority of cataloged objects. By leveraging a third-order extension of Cook's theory, the proposed approach significantly enhances accuracy compared to classical MOID methods while maintaining high computational efficiency. Extensive validation using real RSOs from the Space-Track catalog confirms the method's effectiveness in accurately estimating the minimum distance between perturbed orbits, providing a reliable tool for conjunction analysis and space traffic management.

Keywords: Astrodynamics; MOID.

1. INTRODUCTION

The minimum distance between any two points on two osculating orbits is widely used to assess potential close approaches and collision risks between artificial space objects. By providing a measure of the minimum possible separation between two osculating orbits, the MOID serves as a fundamental tool for conjunction analysis. As the number of objects in Earth's orbit continues to grow (including both operational satellites and space debris) there is an increasing need for swift and reliable methods to compute the MOID efficiently.

The problem of computing the minimum distance between two Keplerian orbits has been extensively studied in the literature [6, 7, 9, 10, 8, 19]. The MOID, defined as the absolute minimum of this function, has been employed in the so-called *orbit-path* filter, which relies on this distance for preliminary screening. While Keplerian-based MOID computation methods can be applied to perturbed orbits by using osculating orbital elements, they often fail to provide an accurate estimation of the true minimum distance between two perturbed orbits (here called "true" MOID). The limitations of purely Keplerian approaches applied in conjunction analysis have been noted in previous studies [11, 20].

Extending the work in [16], a new conjunction filter that addresses the shortcomings of these techniques by incorporating the effects of the zonal harmonics of the geopotential, has been proposed in [15]. The filter is conceived for RSOs in LEO with eccentricities smaller than 0.1, and for RSOs pairs with mutual inclinations in the range [10, 170] degrees, so that the points realizing the MOID are very close to or coinciding with the mutual nodes [6]. The proposed procedure provides a more accurate and reliable MOID estimation of pairs of perturbed orbits for a screening time of 5 days, while maintaining high computational efficiency.

The method proposed in [15] is effective for filtering purposes, but can be overly conservative in MOID computation. Here, that method is improved to devise an effective non-Keplerian MOID assessment tool. The new tool has been extensively validated with a large dataset and compared against existing approaches in the literature.

The structure of this paper is as follows: Section 2 defines the true MOID for perturbed orbits and discusses the inadequacy of the Keplerian osculating MOID in this context. Section 3 details the proposed non-Keplerian MOID assessment tool and Section 4 presents validation tests and a performance comparison against the Keplerian osculating MOID. Finally, Section 5 summarizes the findings and outlines potential directions for future research.

Proc. 9th European Conference on Space Debris, Bonn, Germany, 1–4 April 2025, published by the ESA Space Debris Office
Editors: S. Lemmens, T. Flohrer & F. Schmitz, (http://conference.sdo.esoc.esa.int, April 2025)

2. TRUE VS. KEPLERIAN OSCULATING MOID

Let us consider two RSOs whose (non-Keplerian) trajectories are characterized by the position vectors $\mathbf{r}_A(t)$ and $\mathbf{r}_B(t)$ over a time interval $I = [t_0, t_0 + \varDelta t]$ of interest. The duration $\varDelta t$ can be thought of as the time horizon of a conjunction screening process, which typically lasts a few days. From a theoretical point of view, one can consider the (true) minimum orbit intersection distance between the two RSOs over the interval I by computing the absolute minimum of all the distances between any two of their respective points with no regard to phasing as:

$$\mathrm{true\,MOID}'\,(t_0, \Delta t) = \min_{t_A, t_B \in I} \|\mathbf{r}_B(t_B) - \mathbf{r}_A(t_A)\|\,.$$

Because having a true MOID smaller than the combined physical size of both objects is a necessary condition for a collision to occur, the preceding quantity is of great interest in the process of conjunction screening and filtering. This is especially true if one considers that *phasing* errors (errors in the timing of when objects reach specific points in their orbits, reflected by along-track position uncertainties) are typically the dominant component of an RSO uncertainty distribution volume.

Nevertheless, completely disregarding the phasing information for the two RSOs is unrealistic as phasing errors are typically much smaller than the full width of the conjunction screening window. Hence, a more practical definition of true MOID can be given after limiting the maximum phasing difference of each pair of points to less than the greater of the two orbit periods, T_A and T_B, computed at t_0 :

$$\mathrm{true\,MOID}\,(t_0, \Delta t) = \min_{\substack{t_A, t_B \in I \\ |t_B - t_A| \le \max(T_A, T_B)}} \|\mathbf{r}_B(t_B) - \mathbf{r}_A(t_A)\|\,.$$

The preceding definition will be employed as standard for the analysis conducted in the present article. An alternative approach for measuring the distance between two perturbed orbits consists in computing the MOID of the osculating Keplerian trajectories at times t_k, $k = 0, \ldots, m$. This can be done through highly efficient MOID computation tools available in the literature [e.g., 8]. It results a time-dependent Keplerian osculating MOID, where the minimum value is often used as a proxy for the true MOID [see, for instance, 1, 4, 3]. However, as demonstrated in the following examples, the presence of gravitational perturbations causes the osculating MOID function to significantly underestimate the true MOID in LEO, making it an unreliable metric for accurate conjunction assessment.

Fig. 1 illustrates the time evolution of the Keplerian osculating MOID over 5 days for two pairs of space objects. The initial conditions are detailed in Tab. 1 and the computations are carried out using a high-fidelity dynamical model[1]. As depicted in the figure, the osculating MOID function reaches zero multiple times in both scenarios. However, the numerically computed true MOID values remain considerably above zero, measuring 22.97 km and 9.58 km, respectively. These findings suggest that Keplerian MOID calculations are often overly conservative, emphasizing the necessity of a non-Keplerian approach.

RSO (NORAD)	41732	42775	41460
a (km)	6,839.44	6,867.10	6,875.36
e	0.0023	0.0019	0.0125
i (deg)	97.36	97.20	98.27
ω (deg)	120.14	139.31	129.61
Ω (deg)	229.73	339.11	129.53

Table 1. Osculating orbital elements at epoch JD 2,459,885.88 for the RSOs considered in Fig. 1.

3. NON-KEPLERIAN MOID ASSESSMENT TOOL

The proposed method for estimating a non-Keplerian MOID enhances previous approaches by explicitly accounting for perturbations of the geopotential zonal harmonics over a defined time window. It builds upon the space occupancy path filter developed in [15], employing that procedure to compute the boundaries of the orbital altitude at the mutual nodes. These altitudes are then compared to determine the minimum separation distance. A summary of the procedure implemented to estimate the orbital altitude at the mutual nodes is provided below.

The algorithm is formulated as an optimization problem aimed at computing the maximum and minimum values of the orbital radius as a function of two variables over a compact domain. An analytical expression for the radius is derived in Section 3.1. Section 3.2 describes the computation of the argument of latitude interval that defines the positions of the mutual nodes. Section 3.3 explains how to solve the optimization problem and determine the radial boundaries, and Section 3.4 details the computation of the minimum distance. Finally, Section 3.5 introduces a sampling method which is necessary to improve the accuracy.

3.1. Analytical expression for the orbital radius

An analytical expression for the orbital radius is derived by accounting for short-period effects driven by the J_2 zonal harmonic, while neglecting higher-order contributions. Since the maximum target eccentricity is 0.1, the expansion is carried out up to the third order in eccentricity. Employing a classical result [see 17], the orbital

[1] This numerical propagation model incorporates a 23×23 geopotential representation, accounts for luni-solar third-body perturbations, and includes corrections for Earth's geoid precession and nutation.

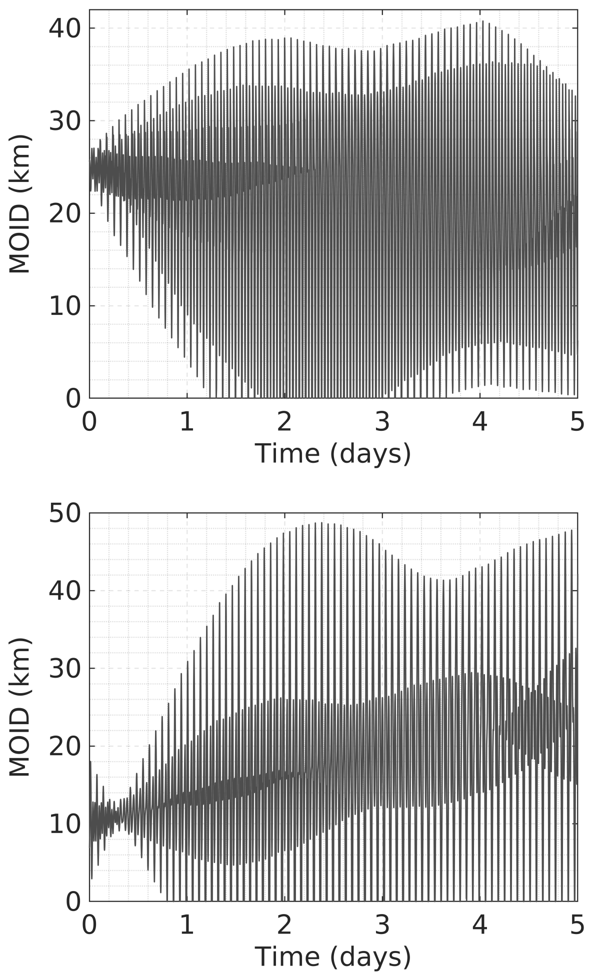

Figure 1. Keplerian osculating MOID for the two pairs of objects NORAD 41732, NORAD 42775 (above) and NORAD 41732, NORAD 41460 (below).

radius is approximated as

$$r \simeq a \left[1 - e \cos M + \frac{1}{2} e^2 (1 - \cos 2M) + \frac{3}{8} e^3 (\cos M - \cos 3M) \right].$$

In this formula, the orbital elements *a*, *e*, and *M* are decomposed into their mean values ($\hat{a}$, $\hat{e}$, $\hat{M}$) and short-period variations, which are calculated using the equations derived by Kozai [12] and Lyddane [14]. After some algebraic manipulations, the radius is expressed in terms of the mean elements as

$$r \simeq \hat{a}\big(1 - \hat{e}\cos(\hat{\theta} - \hat{\omega})\big)\big(1 - \hat{e}^2 \sin^2(\hat{\theta} - \hat{\omega})\big) + \frac{J_2}{4\hat{a}}\big[\big(9 + \cos 2\hat{\theta}\big)\sin^2 \hat{i} - 6\big], \tag{1}$$

where $\hat{\theta}$ is the mean argument of latitude. Here, $\hat{a}$ and $\hat{i}$ are assumed constant because zonal harmonics do not induce long-period and secular variations in these elements, in contrast to $\hat{e}$ and $\hat{\omega}$. The evolutions of $\hat{e}$ and $\hat{\omega}$ are represented by an extension of Cook's theory [5] as refined in [15] to include the dominant nonlinear effects of order $J_2 \hat{e}^2$. Let

$$\xi = \hat{e}\cos\hat{\omega}, \qquad \eta = \hat{e}\sin\hat{\omega} \tag{2}$$

be the mean eccentricity vector nodal components. Their evolution with respect a non-dimensional time τ are given by [see 15]

$$\begin{cases} \xi(\tau) = e_p \cos\left(\kappa_\xi \kappa\, \tau + \alpha\right), \\ \eta(\tau) = \kappa e_p \sin\left(\kappa_\xi \kappa\, \tau + \alpha\right) + e_f, \end{cases} \tag{3}$$

where

$$\kappa = \sqrt{\frac{\kappa_\eta}{\kappa_\xi}}.$$

The quantities e_p, e_f, which represent the *proper* and *frozen* eccentricity, respectively, κ_ξ, κ_η, and α are constant and are defined in [15]. Let us introduce the angle β for the argument appearing in the expressions of $\xi(\tau)$ and $\eta(\tau)$ in (3):

$$\beta(\tau) = \kappa_\xi \kappa\, \tau + \alpha, \tag{4}$$

which will play the role of the time variable.

Over a 5-days interval, while the fast angle $\hat{\theta}$ cycles multiple times within $[0, 2\pi)$, β changes only slightly. This separation of time scales allows us to assume that r is a function of the two independent variables β and $\hat{\theta}$. The final expression for $r(\hat{\theta}, \beta)$ is obtained by using in (1) the definitions (2) and the solutions (3), yielding

$$\begin{aligned} r \simeq\ & \hat{a}\big(1 - e_p \cos\beta \cos\hat{\theta} - \kappa e_p \sin\beta \sin\hat{\theta} - e_f \sin\hat{\theta}\big) \cdot \\ & \Big[1 - \big(e_p \cos\beta \sin\hat{\theta} - \kappa e_p \sin\beta \cos\hat{\theta} - e_f \cos\hat{\theta}\big)^2\Big] \\ & + \frac{J_2}{4\hat{a}}\big[\big(9 + \cos 2\hat{\theta}\big)\sin^2 \hat{i} - 6\big]. \end{aligned} \tag{5}$$

3.2. Computation of the intervals $\mathcal{T}$, $\mathcal{T}^*$

The locations of the mutual nodes are determined by their arguments of latitude, which are computed as follows. The latitude of one of the two pairs of mutual nodes is given by[2]

$$\phi = \arcsin\left(\frac{\sin\hat{i}_1 \sin\hat{i}_2 \sin\Delta\hat{\Omega}}{\sin\gamma}\right),$$

where $\hat{i}_1$, $\hat{i}_2$ are the mean inclinations of the two orbital planes, $\Delta\hat{\Omega} = \hat{\Omega}_2 - \hat{\Omega}_1$, and the mutual inclination γ, which is defined as the angle between the directions orthogonal to the orbital planes, is found from the relation

$$\gamma = \arccos\big(\cos\hat{i}_1 \cos\hat{i}_2 + \sin\hat{i}_1 \sin\hat{i}_2 \cos\Delta\hat{\Omega}\big).$$

[2] The latitude of the other pair is equal to $-\phi$.

If $\hat{i}_1\hat{i}_2 \neq 0$, the arguments of latitude of the mutual nodes are computed from

$$\sin\hat{\theta}_k = \frac{\sin\phi}{\sin\hat{i}_k}, \qquad k = 1, 2, \tag{6}$$

which admits two solutions in $[0, 2\pi)$. The ambiguity can be resolved as detailed in [15] by analyzing the projection of the orbit over a non-rotating Earth in the inertial reference frame.

Since the quantity $\Delta\hat{\Omega}$ shows long-period and secular variations due to the geopotential, the arguments of latitude $\hat{\theta}_1$ and $\hat{\theta}_2$ of the mutual nodes also change with time. Thus, it is necessary to compute for each object of the pair the ranges of variation $\mathcal{T}_k$, $\mathcal{T}_k^*$, $k = 1, 2$, of the arguments of latitude of the two mutual nodes in the time interval I of interest:

$$\mathcal{T}_k = [\hat{\theta}_{\min,k}, \hat{\theta}_{\max,k}],$$
$$\mathcal{T}_k^* = [\hat{\theta}_{\min,k} + \pi, \hat{\theta}_{\max,k} + \pi].$$

The values $\hat{\theta}_{\min,k}$ and $\hat{\theta}_{\max,k}$ are determined depending on whether $\hat{\theta}_k(\tau)$ is monotonic or has a critical point (either maximum or minimum) in I. All the details about the computation of these intervals are given in [15].

3.3. Orbital radius bounds

This section presents an efficient method for determining the minimum and maximum values taken by the orbital radius $r(\hat{\theta}, \beta)$ at the mutual nodes within each domain $\mathcal{D}$, $\mathcal{D}^*$, defined as

$$\mathcal{D} = \mathcal{T} \times \mathcal{B}, \qquad \mathcal{D}^* = \mathcal{T}^* \times \mathcal{B},$$

where

$$\mathcal{B} = [\beta_{\min}, \beta_{\max}],$$

with $\beta_{\min} = \beta(t_0)$ and $\beta_{\max} = \beta(t_0 + \Delta t)$ (see 4).

The absolute and local minima/maxima of $r(\hat{\theta}, \beta)$ in the domain $[0, 2\pi) \times \mathbb{R}$ are searched for by a simplified approach for saving computational time. Four critical points of $r(\hat{\theta}, \beta)$ can be easily identified: $(\pi/2, \pi/2)$, $(\pi/2, 3\pi/2)$, $(3\pi/2, \pi/2)$, $(3\pi/2, 3\pi/2)$. Additional critical points to these four, which may appear only if the frozen and proper eccentricities, and thus $\hat{e}$, are sufficiently small, are obtained for a simpler expression of $r(\hat{\theta}, \beta)$ than the right-hand side of (5) (see [15]).

If the absolute minimum/maximum point lies within $\mathcal{D}$ ($\mathcal{D}^*$), the corresponding value of r is computed by (5). Otherwise, it is necessary to search for the absolute minimum/maximum of r on the border of $\mathcal{D}$ ($\mathcal{D}^*$), checking at the same time whether the interior of $\mathcal{D}$ ($\mathcal{D}^*$) contains local minima/maxima points. The search for minima/maxima points of $r(\hat{\theta}, \beta)$ on the border of $\mathcal{D}$ ($\mathcal{D}^*$) is done by computing the critical points of the functions

$$r_{\beta_*}(\hat{\theta}) = r(\hat{\theta}, \beta_*),$$
$$r_{\hat{\theta}_*}(\beta) = r(\hat{\theta}_*, \beta),$$

for suitable values of $\hat{\theta}_*$, β_*. By setting their derivatives equal to zero yields two polynomial equations of degree six.

3.4. Non-Keplerian MOID

Denote the minimum and maximum orbital radii in the domains $\mathcal{D}_k$ and $\mathcal{D}_k^*$ as $r_{\min,k}$, $r_{\max,k}$ and $r^*_{\min,k}$, $r^*_{\max,k}$, respectively (where $k = 1, 2$ refers to each object of the pair) and introduce the following intervals:

$$\mathcal{R}_k = [r_{\min,k}, r_{\max,k}],$$
$$\mathcal{R}_k^* = [r^*_{\min,k}, r^*_{\max,k}].$$

If

$$\mathcal{R}_1 \cap \mathcal{R}_2 \neq \emptyset \quad \vee \quad \mathcal{R}_1^* \cap \mathcal{R}_2^* \neq \emptyset,$$

at least two radial intervals relative to one mutual node overlap and the non-Keplerian MOID is set equal to zero. Otherwise, if

$$\mathcal{R}_1 \cap \mathcal{R}_2 = \emptyset \quad \wedge \quad \mathcal{R}_1^* \cap \mathcal{R}_2^* = \emptyset,$$

the non-Keplerian MOID is set equal to $\min\{d, d^*\}$, where

$$d = \max\{r_{\min,1} - r_{\max,2}, r_{\min,2} - r_{\max,1}\},$$
$$d^* = \max\{r^*_{\min,1} - r^*_{\max,2}, r^*_{\min,2} - r^*_{\max,1}\}.$$

3.5. Time interval sampling

The developed algorithm tends to provide a rather conservative estimate of the minimum distance between the two objects. This is particularly evident when one orbit exhibits moderate eccentricity and a relatively fast motion of the ascending node. In such cases, the range of values taken by the orbital radius for a fixed argument of latitude that belongs to $\mathcal{B}$ is quite large (see Fig. 3). Moreover, the size of the interval $\mathcal{T}$ can vary significantly. If the rates of the ascending nodes of both orbits are similar, this interval measures only a few tenths of a degree. However, if the absolute value of the difference between the two frequencies is large, $\mathcal{T}$ can extend up to several degrees. In this case, the domain $\mathcal{D} = \mathcal{T} \times \mathcal{B}$ is quite large, leading to highly conservative bounds of the orbital radius.

The pair NORAD 1778 and NORAD 27597 exemplifies this scenario. The initial conditions of the two objects are presented in Tab. 2. Fig. 2 shows both orbits in Cartesian coordinates over a 5-days interval. Fig. 3 shows the evolution of NORAD 1778's radius as a function of the argument of latitude. This satellite has an eccentricity of ≈ 0.07 and a regression rate of the ascending node of

RSO (NORAD)	1778	27597
a (km)	7,462.31	7,166.43
e	0.0748	0.0026
i (deg)	34.33	98.51
ω (deg)	229.12	97.07
Ω (deg)	143.75	247.98

Table 2. Osculating orbital elements at epoch JD 2,459,885.88 for the RSOs considered in Fig. 1.

≈ -0.2 deg/h. Fig. 4 shows the corresponding evolution for NORAD 27597, whose orbit is much less eccentric and is characterized by a precession rate of the ascending node of ≈ 0.04 deg/h. As a result, the intervals $\mathcal{T}_k$, $\mathcal{T}_k^*$, $k = 1, 2$, of the argument of latitude of the mutual nodes are quite large, particularly for NORAD 1778, where the range of values of the orbital radius for a constant $\hat{\theta} \in \mathcal{T}_k, \mathcal{T}_k^*$ is also quite broad.

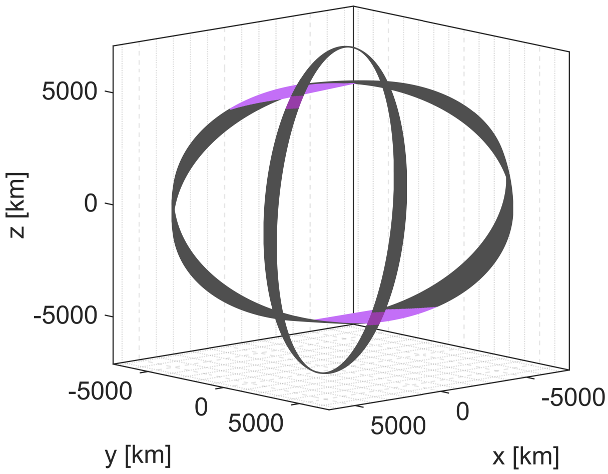

Figure 2. Orbits of NORAD 1778 and NORAD 27597 for a time duration of 5 days. Light and dark purple points refer to points of the propagated orbits whose values $(\hat{\theta}, \beta)$ belong to the domains $\mathcal{D}$ and $\mathcal{D}^*$ as computed by the proposed procedure without applying any sampling of the 5 days interval.

This pair reaches the minimum distance at the mutual node located in the Southern hemisphere[3]. The maximum and minimum values of the orbital radius at this node for each orbit as computed from the proposed algorithm are reported in Tab. 3. One can observe that the radius of NORAD 27597 varies by less than 1 km, whereas that of NORAD 1778 changes by more than 350 km. Since the ranges of values covered by the orbital radius of the two objects overlap, the non-Keplerian MOID is set equal to zero. However, the numerically estimated true MOID remains significantly above zero, at 118.44 km.

[3]The intervals of variation of the argument of latitude of this mutual node, as obtained from the proposed procedure, are $[276.82, 303.30]$ deg for NORAD 1778 and $[208.42, 214.44]$ deg for NORAD 27597, where the values of the extrema have been rounded to the second decimal digit.

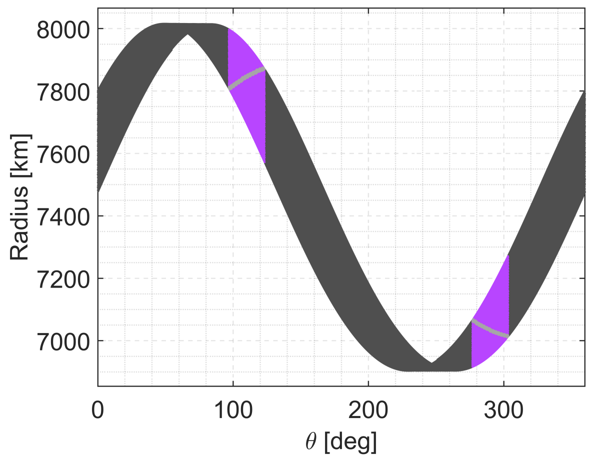

Figure 3. Orbital radius of NORAD 1778 versus the argument of latitude. The meaning of the purple dots is the same as in Fig. 2. The purple dots are replaced by the gray dots if a sampling interval of 30 minutes is applied.

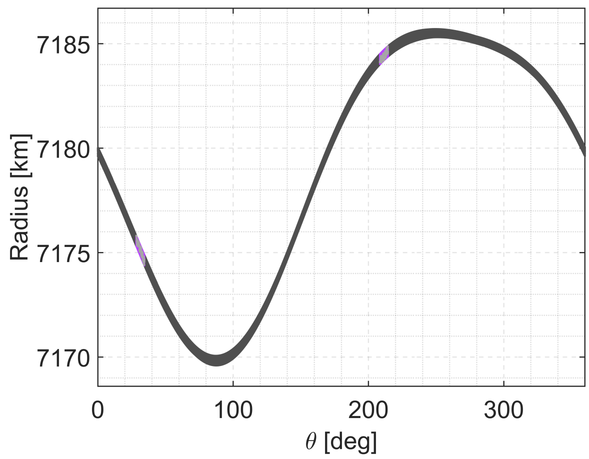

Figure 4. Same as Fig. 3 but for the object NORAD 27597.

This significant underestimation of the minimum distance can be mitigated by analyzing smaller time intervals. If the size of the interval $\mathcal{B}$ is reduced, also the intervals $\mathcal{R}$, $\mathcal{R}^*$ become smaller, as well as $\mathcal{T}$, $\mathcal{T}^*$. Therefore, rather than computing the non-Keplerian MOID for the whole duration Δt of 5 days, one can compute it several times from t_0 to $t_0 + \Delta t$. While increasing the number of intervals improves accuracy, it also increases computational time. As a trade-off, the procedure is run every 30 minutes during the 5 days.

The benefit produced by this strategy (which was not presented in [15]) is particularly important for the object NORAD 1778, as can be appreciated from Fig. 3 and Tab. 4. From this table one can see that the range of values of the orbital radius at the mutual node in the Southern hemisphere has decreased of 60 km (see also Tab. 3). On the other hand, the impact on NORAD 27595 is al-

RSO (NORAD)	1778	27597
$r_{\max}$ (km)	7,270.85	7,184.88
$r_{\min}$ (km)	6,916.23	7,184.02

Table 3. Maximum and minimum values of the orbital radius at the mutual node located in the Southern hemisphere for NORAD 1778 and NORAD 27597 as computed by the proposed procedure without applying any sampling of the 5 days interval.

RSO (NORAD)	1778	27597
$r_{\max}$ (km)	7,069.57	7,184.87
$r_{\min}$ (km)	7,010.24	7,184.09

Table 4. Same as in Tab. 3 but by applying a sampling interval of 30 minutes.

most negligible as expected, because $r_{\max} - r_{\min}$ was already smaller than 1 km.

By computing the non-Keplerian MOID every 30 minutes, the evolutions of the extrema that define the intervals $\mathcal{R}_k$, $\mathcal{R}_k^*$ can be known during the 5-days duration or until a conjunction is detected. Fig. 5 (left) shows how these values evolve for the mutual node in the Southern hemisphere of the pair under consideration, while Fig. 5 (right) shows for the same pair the evolution of the non-Keplerian MOID computed every 30 minutes. The minimum of all these values, which gives the non-Keplerian MOID for a time duration of 5 days, is attained at the initial epoch and is equal to 118.09 km, reducing the error from 118.44 km to only 0.35 km.

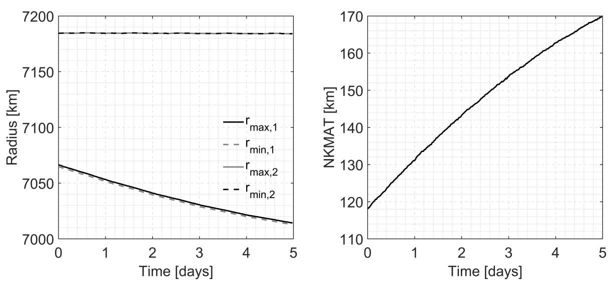

Figure 5. Evolution of the maximum and minimum orbital radius of NORAD 1778 and NORAD 27597 at the mutual node in the Southern hemisphere (left) and the corresponding non-Keplerian MOID (right) computed every 30 minutes.

4. RESULTS

The NKMAT developed in this work to compute the minimum distance between two non-Keplerian orbits has been tested and validated against 272,240 pairs selected from a subset of the dataset used in [15]. That study built a dataset of 16,951 orbits from the publicly available Two-Line Element sets (TLEs) and processed them using the SGP4 theory [18]. This dataset was obtained by removing orbits with an eccentricity higher than 0.1 and an apogee radius exceeding 40,000 km. Additionally, orbits with inclinations below 0.06 deg were excluded (21 orbits in total).

All orbits in the dataset were propagated to a common epoch t_0 (11/02/2022, 09:18:20) and then propagated forward for 5 days. The dynamical model employed for this propagation includes a 23×23 geopotential along with luni-solar third-body perturbations and accounts for Earth's geoid precession, nutation, and polar motion effects. Earth orientation, the values of the harmonic coefficients, and the positions of the Sun and Moon are obtained from the corresponding SPICE kernels. Note that the NKMAT is based on a dynamical model that only considers zonal harmonics of the geopotential and assumes that Earth's polar axis is aligned with the z-axis of the J2000 inertial frame.

The pairs used in this validation were randomly chosen from the 32,474,006 pairs identified in [15]. Initially, 500,000 pairs were selected, and among them, only those with a true MOID smaller than 30 km were retained, because the accuracy of this calculation becomes more relevant in these cases. Moreover, note that the NKMAT can only be applied to pairs with a mutual inclination in the range [10, 170] deg.

For the validation conducted in this work, the true MOID is computed as explained in Section 2. The trajectories used as ground truth are those obtained from the numerical propagation with a time resolution of 5 s. However, due to the high speeds of objects in LEO, this resolution is not sufficient for an accurate approximation of the true MOID. Thus, around the points where the minimum values of the distance are reached, the resolution is increased to 0.02 s, using linear interpolation with the generalized equinoctial orbital elements [2]. Section 4.1 presents the results of the NKMAT compared to the ground truth.

Additionally, the outcome of the NKMAT is compared with the Keplerian osculating MOID evaluated every 25 s using the osculating orbital elements obtained from the numerical propagation. The results of this comparison are presented in Section 4.2.

4.1. Results of the NKMAT

The performance of the NKMAT is evaluated through the error ϵ defined as the difference between the true MOID, considered as ground truth, and the minimum distance computed by our tool:

$$\epsilon = (\text{true MOID}) - (\text{non-Keplerian MOID}). \quad (7)$$

Note that while a positive error leads to an underestimation of the minimum value and thus to a false alarm, a negative error can lead to a miss-detection of a collision.

Fig. 6 presents the histogram and cumulative density function of ϵ. This graph highlights the outstanding ac-

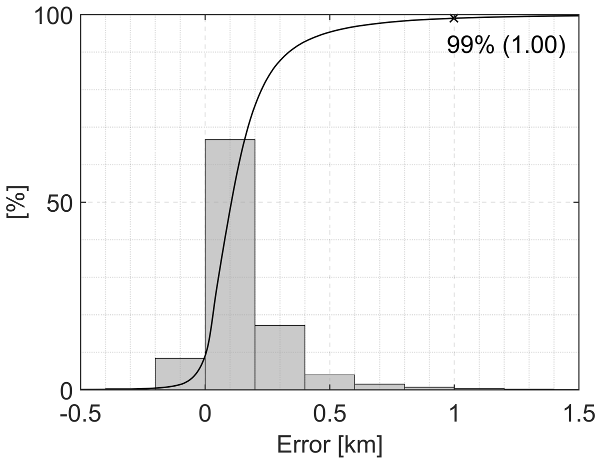

Figure 6. Histogram and cumulative density function of the errors of the NKMAT as defined in (7)*.*

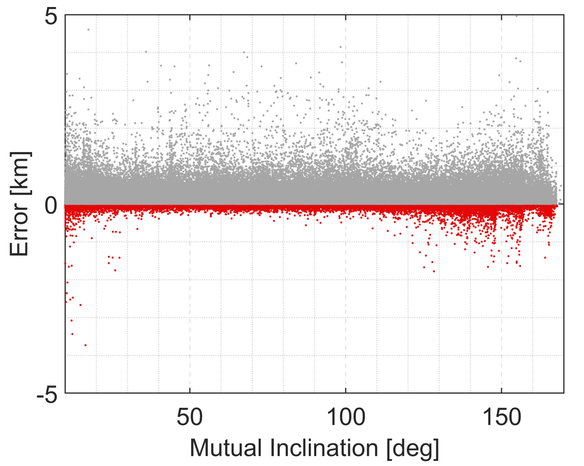

Figure 7. Errors of the NKMAT as defined in (7) *versus the mutual inclination (computed at the initial time).*

curacy of the proposed tool. In 99% of the cases, the error remains below 1 km, demonstrating the method's reliability in estimating the minimum distance. Moreover, more than 65% of the cases exhibit an error between 0 and 0.2 km, further confirming the precision of the approach. Importantly, only 9% of the cases show a negative error, which means an underestimation of the true minimum distance. However, these cases are still well controlled, as merely 0.02% of the total cases present a negative error smaller than -1 km. These results underscore the robustness of the NKMAT in capturing the true MOID with high fidelity, even in complex non-Keplerian conditions.

The method is built on two main assumptions: the minimum distance is realized by points that are close to the mutual nodes (since the orbital planes of any pair of objects are far from being coplanar) and the eccentricity is small, allowing the orbital radius to be well-approximated by the expression in (5).

To better characterize the error, particularly the negative ones, Fig. 7 shows the values of ϵ versus those of the mutual inclination. It can be observed that the most negative errors occur for small mutual inclinations. On the other hand, positive errors do not show a clear dependence on the mutual inclination. Concerning the second assumption, Fig. 8 shows the errors ϵ versus the maximum eccentricity of the two orbits of the pair evaluated at the initial time. As expected, larger values of this orbital element lead to greater positive and smaller negative errors in the non-Keplerian MOID.

To reduce the occurrence of negative errors, which are mainly due to values of the mutual inclination close to 10 and 170 deg, these bounds have been changed to 17 and 163 deg, respectively. This adjustment reduces the number of considered pairs of approximately 6.4%. With this restriction, the minimum negative error is higher than -1 km for pairs whose eccentricities are smaller than 0.04, whereas for more eccentric orbits, the negative error can

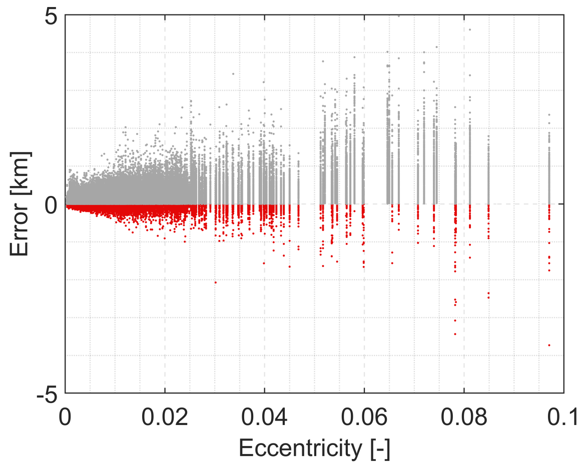

Figure 8. Errors of the NKMAT as defined in (7) *versus the largest among the two eccentricities (computed at the initial time).*

reach -2 km. Fig. 9 shows the errors versus the maximum eccentricity of the two orbits of the pair evaluated at the initial time for the reduced population of pairs.

4.2. Comparison with the osculating MOID

Section 2 explains that the osculating MOID provides a poor estimation of the true MOID in LEO due to the effect of gravitational perturbations, as exemplified by two particular cases. Fig. 10 presents the histograms of the values of the true and osculating MOID for all the pairs in the reduced population (254,703 pairs). While around 20% of the cases present a true MOID smaller than 1 km, for more than 90% of the pairs the osculating MOID is below 1 km, resulting in a high rate of false alarms.

To further highlight the different behaviors of the oscu-

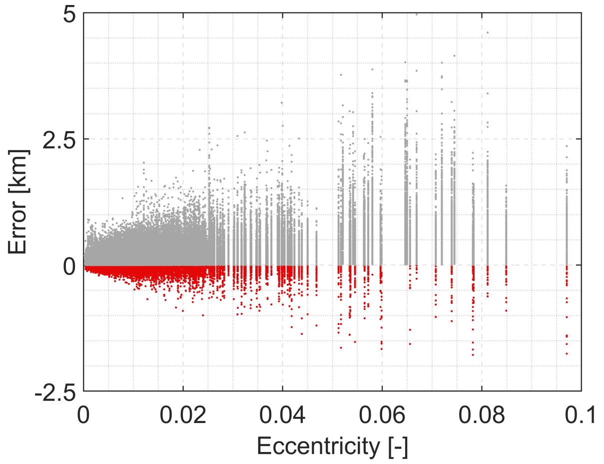

Figure 9. Same as Fig. 8 but for those pairs whose initial mutual inclination belongs to the interval [17, 163] deg (instead of [10, 170] deg).

lating and non-Keplerian MOID as compared to the true MOID, Fig. 11 displays the results for three specific pairs of objects: (NORAD 33913, NORAD 34571), (NORAD 42167, NORAD 12663), and (NORAD 12737, NORAD 10991). The initial orbital elements of the six objects are reported in Tab. 5. It is evident that the non-Keplerian MOID as computed by the new tool closely follows the true MOID over the 5 days. In contrast, the oscillatory behavior of the osculating MOID obscures the true minimum, making it less reliable for capturing the actual minimum distance.

To generalize the comparison, the osculating MOID was also computed for the reduced population of pairs. Since the error in the osculating MOID is strongly correlated with the magnitude of the true MOID, six histograms relative to different ranges of the true MOID are presented in Fig. 12 for the error

$$\epsilon_{osc} = (\text{true MOID}) - (\text{osculating MOID}). \quad (8)$$

It is worth noting that the osculating MOID exhibits errors of the same order of magnitude as the values taken by the true MOID. In cases where the true MOID is between 5 and 10 km, only 0.6% of instances have an error smaller than 5 km; for true MOIDs between 10 and 15 km and between 15 and 20 km, the percentages of cases with errors smaller than the true MOID are 1.96% and 3.87%, respectively. This poor performance arises because most osculating MOID estimates are either zero or very close to zero. For true MOIDs exceeding 25 km, a higher percentage of cases have errors below 25 km, although this still remains under 50%.

Finally, Fig. 13 shows the analogous results for the errors of the non-Keplerian MOID computed by our tool. All histograms exhibit a similar shape, with 99% of the errors around 1 km. These results underscore the robustness of the non-Keplerian MOID assessment tool in accurately capturing the true MOID even under complex

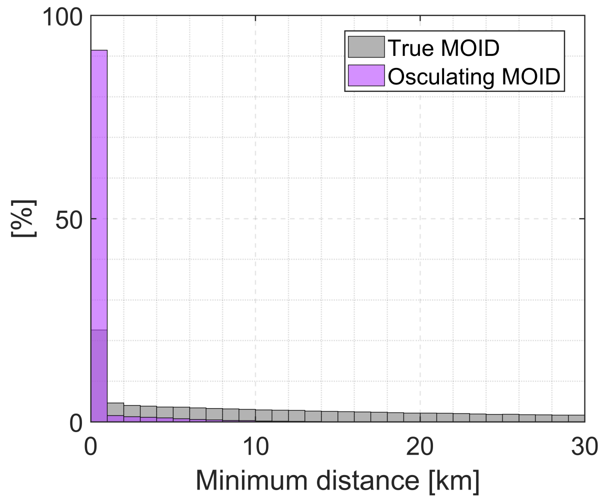

Figure 10. Histogram of the values of the true MOID and the osculating MOID.

non-Keplerian conditions, thereby validating the method as a highly reliable tool for minimum distance estimation.

5. CONCLUSIONS AND FUTURE WORK

This work introduces a fast and accurate method, named non-Keplerian MOID assessment tool, for estimating the minimum distance between two non-coplanar RSOs in low-Earth orbit with moderate eccentricity. Tracking and computing this minimum distance is crucial for identifying potential collisions between Earth-orbiting satellites. While existing methods for MOID computation have been extensively studied in the literature, they typically assume Keplerian orbits and neglect the effects of perturbations. The proposed approach overcomes this limitation by accurately estimating the minimum distance between two non-Keplerian orbits while explicitly accounting for the zonal harmonics of the geopotential.

The method was validated using a large dataset by comparing its minimum distance estimations with both the true MOID and the Keplerian osculating MOID. The analysis reveals that while the osculating MOID often provides overly conservative estimates (frequently reaching 0 km even when the true MOID is close to the safe distance of 30 km, which was set as the maximum value of the true MOID in our dataset of pairs) the new tool delivers a highly accurate approximation. Specifically, 99% of the cases exhibit an error smaller than 1 km, demonstrating the method's reliability.

Beyond offering a precise minimum distance estimation, the method also captures the temporal evolution of this quantity. This enables accurate predictions of its time evolution and allows for the identification of the exact location of the minimum separation—an advantage over the osculating MOID, which is strongly affected by short-

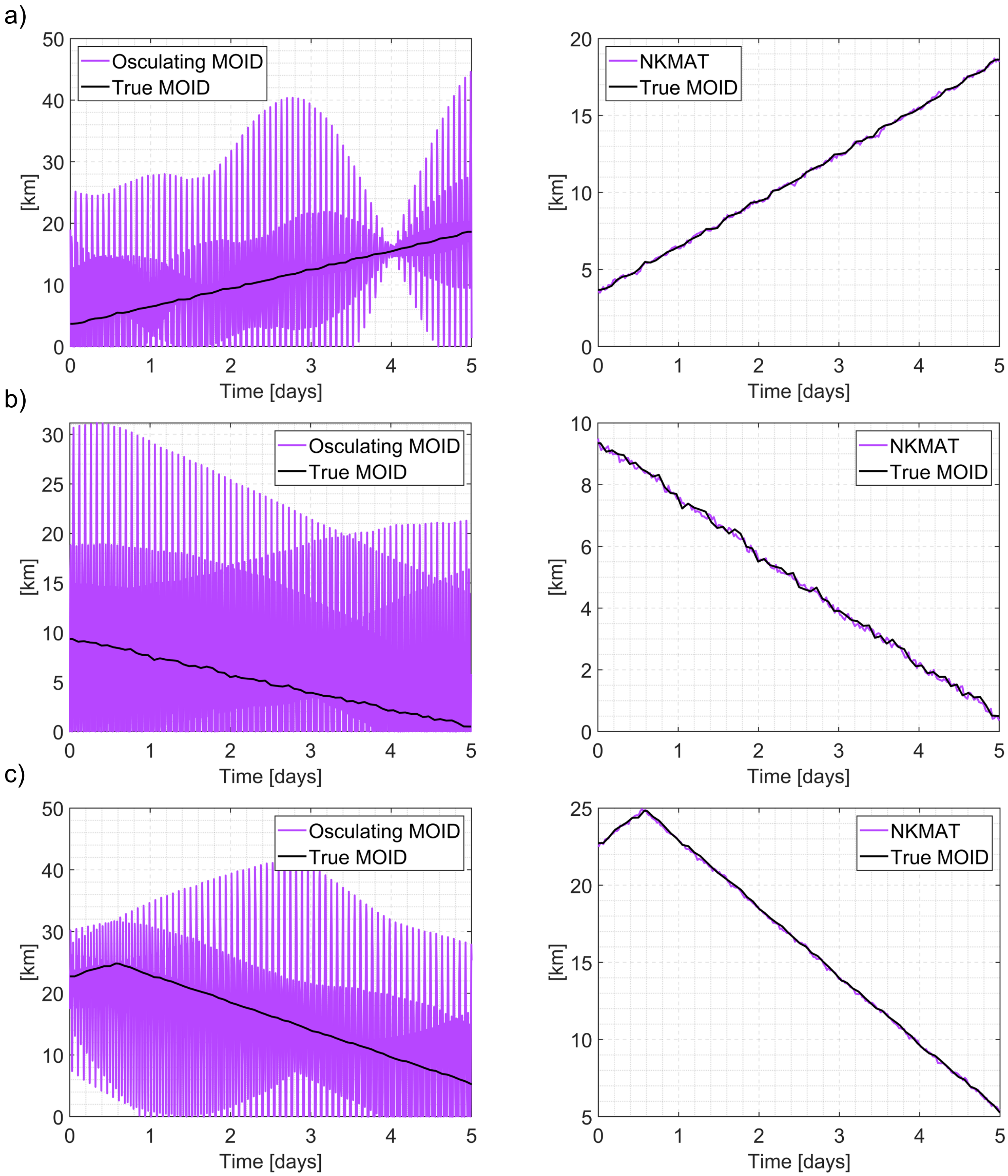

Figure 11. Evolution of the true MOID and the osculating MOID (left) and the true MOID and the non-Keplerian MOID (right) of: a) NORAD 33913, NORAD 34571; b) NORAD 42167, NORAD 12663; c) NORAD 12737, NORAD 10991.

RSO (NORAD)	33913	34571	42167	12663	12737	10991
a (km)	7,126.72	7,193.46	7,335.58	7,324.17	7,384.34	7,360.43
e	0.0067	0.0108	0.0055	0.0051	0.0145	0.0035
i (deg)	74.12	74.18	82.78	83.08	83.02	82.81
ω (deg)	151.44	64.10	334.81	338.35	181.91	110.76
Ω (deg)	138.98	104.27	330.77	77.99	165.64	280.36

Table 5. Osculating orbital elements at epoch JD 2,459,885.88 for the RSOs considered in Fig. 11.

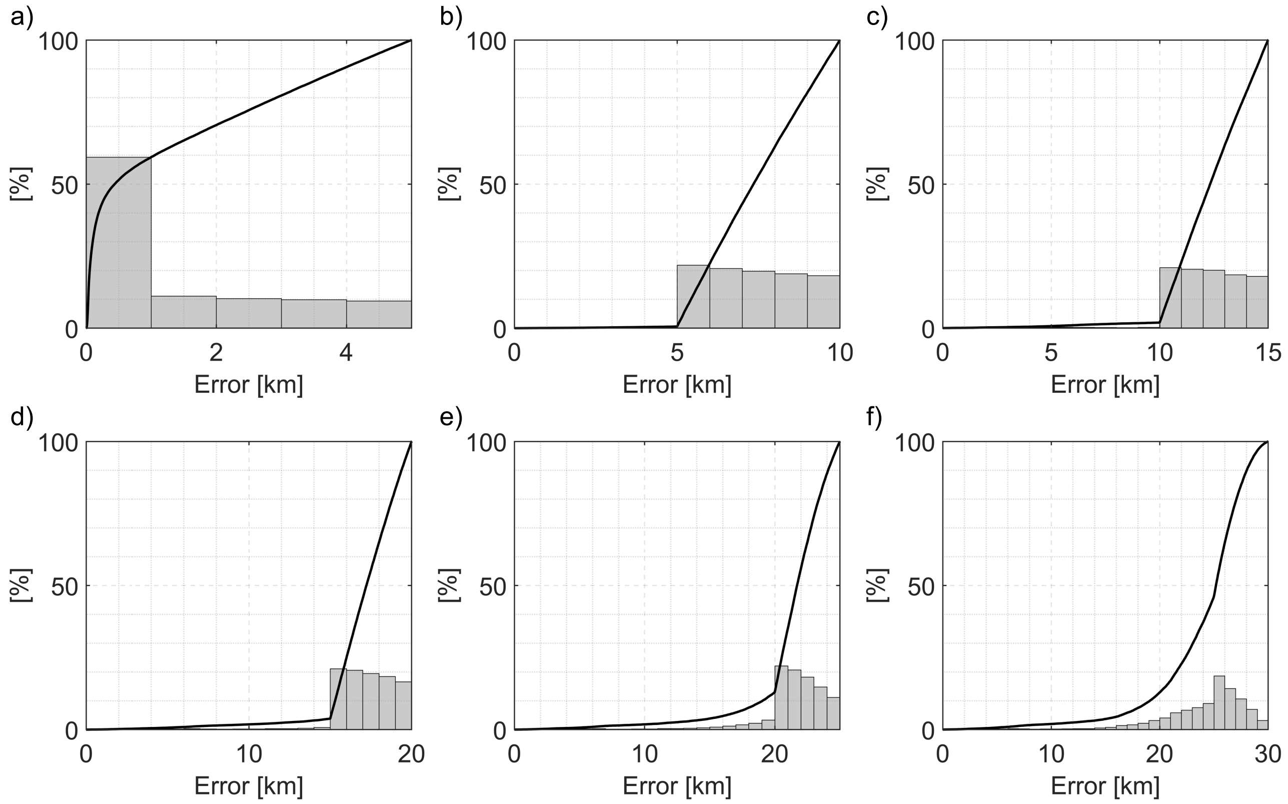

Figure 12. Histograms and cumulative density functions of the errors of the osculating MOID as defined in (8) *for the following ranges of the true MOID: [0, 5] km (a); [5, 10] km (b); [10, 15] km (c); [15, 20] km (d); [20, 25] km (e); [25, 30] km (f).*

period variations and struggles with rapidly evolving orbital configurations. Consequently, this method represents a significant advancement in MOID computation for non-Keplerian trajectories in LEO, establishing itself as a highly reliable tool.

Future work will focus on further refining the NKMAT for cases with low mutual inclination (10 - 20 deg), where the minimum distance can be realized by a pair of points far from the mutual nodes. Additionally, incorporating atmospheric drag and making the procedure accurate also for orbits with higher eccentricities will extend its applicability to the entire LEO region.

ACKNOWLEDGMENTS

The authors gratefully acknowledge support by grant TED2021-132099B-C33 funded by MICIU/AEI/10.13039 /501100011033 and by “European Union NextGenerationEU/PRTR.”. Ana S. Rivero was funded by a FPU grant from the Spanish Ministry of Universities. G. Baù carried out this study within the Space It Up project funded by the Italian Space Agency, ASI, and the Ministry of University and Research, MUR, under contract n. 2024-5-E.0 - CUP n. I53D24000060005.

REFERENCES

1. Alfano S. (2012). Toroidal path filter for orbital conjunction screening. Celestial Mechanics and Dynamical Astronomy, 113(3):321–334.

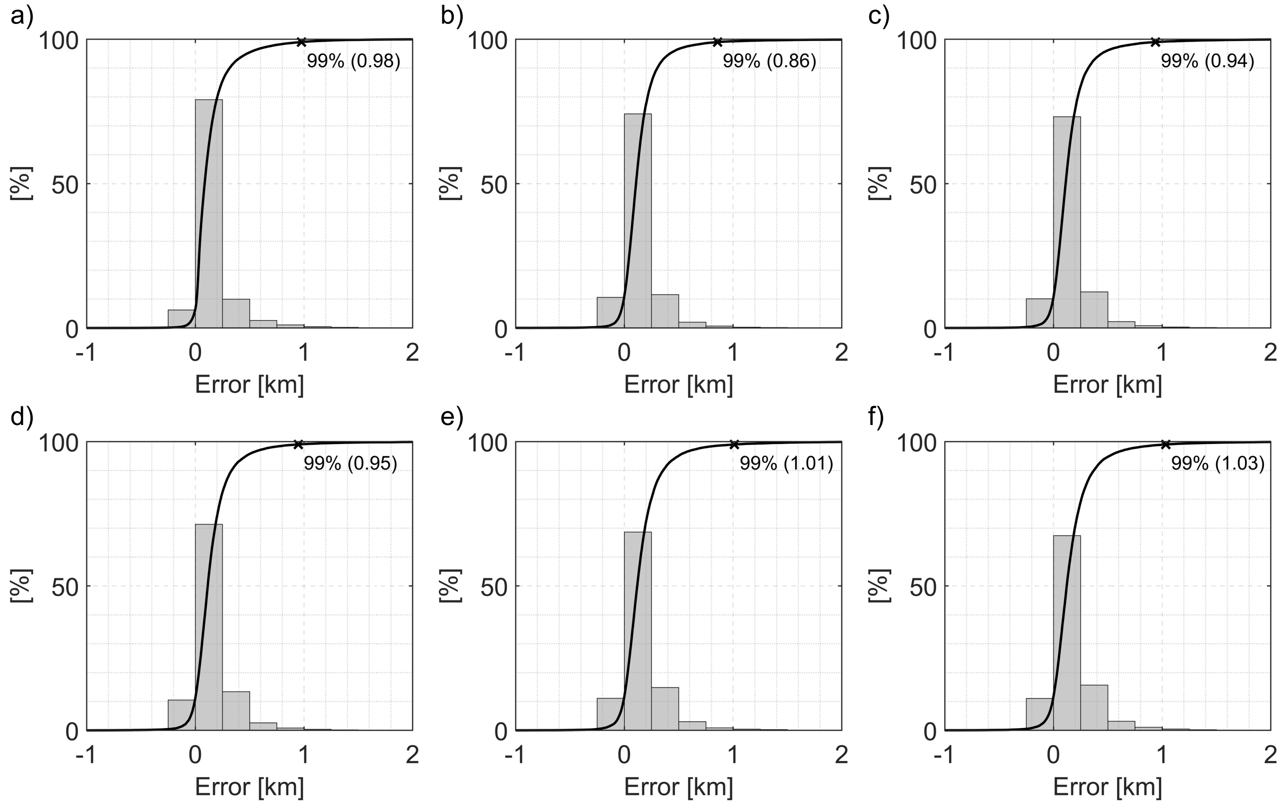

Figure 13. Histograms and cumulative density functions of the errors of the non-Keplerian MOID as defined in (7) *for the following ranges of the true MOID: [0, 5] km (a); [5, 10] km (b); [10, 15] km (c); [15, 20] km (d); [20, 25] km (e); [25, 30] km (f).*

2. Baù G., Hernando-Ayuso J., Bombardelli C. (2021). A generalization of the equinoctial orbital elements. Celestial Mechanics and Dynamical Astronomy, 133, 1-29.

3. Bonaccorsi S., Montaruli M. F., Di Lizia P., Peroni, Panico A., Rigamonti M., and Del Prete F. (2024). Conjunction analysis software suite for space surveillance and tracking. Aerospace, 11(2).

4. Casanova D., Tardioli C., Lemaître A. (2014). Space debris collision avoidance using a three-filter sequence. MNRAS, 442(4):3235–3242.

5. Cook R. A. (1992). The long-term behavior of near-circular orbits in a zonal gravity field. Advances in the Astronautical Sciences, 76:2205–2221.

6. Gronchi G. F. (2003) On the stationary points of the squared distance between two ellipses with a common focus. SIAM Journal on Scientific Computing, 24(1):61–80.

7. Gronchi G. F. (2005). An algebraic method to compute the critical points of the distance function between two Keplerian orbits. Celestial Mechanics and Dynamical Astronomy, 93:295–329.

8. Gronchi G. F., Baù G., Grassi C. (2023). Revisiting the computation of the critical points of the Keplerian distance. Celestial Mechanics and Dynamical Astronomy, 135(5):48.

9. Hedo J. M., Ruíz M., Peláez J. (2018). On the minimum orbital intersection distance computation: a new effective method. MNRAS, 479(3):3288–3299.

10. Hedo J. M., Fantino E., Ruíz M., Peláez J. (2020). Minimum orbital intersection distance: an asymptotic approach. A&A, 633:A22.

11. Hoots F. R., Crawford L. L., Roehrich R. L. (1984). An analytic method to determine future close approaches between satellites. Celestial Mechanics, 33(2):143–158.

12. Kozai Y. (1959). The motion of a close Earth satellite. The Astronomical Journal, 64:367–377.

13. Kozai Y. (1962). Second-order solution of artificial satellite theory without air drag. The Astronomical Journal, 67 (7):446–461.

14. Lyddane R. H. (1963). Small eccentricities or inclinations in the Brouwer theory of the artificial satellite. The Astronomical Journal, 68(8):555–558.

15. Rivero A. S., Baù G., Vazquez R., Bombardelli C. (2024). A novel conjunction filter based on the minimum distance between perturbed trajectories, URL https://arxiv.org/abs/2410.20928.

16. Rivero A. S., Bombardelli C., Vazquez R. (2024). Short-term space occupancy and conjunction filter, URL https://arxiv.org/abs/2309.02379.

17. Smart W. M. (1953). Celestial Mechanics. Longmans, Green & Co.

18. Vallado D. A., Crawford P., Hujsak R., Kelso T. S. (2006). Revisiting spacetrack report# 3: Rev 1. In AIAA/AAS Astrodynamics Specialist Conference and Exhibit, 21-24 August 2006, Keystone, CO.

19. Wisniowski T., Rickman H. (2013). Fast geometric method for calculating accurate minimum orbit intersection distances (MOIDs). Acta Astronaituca 63, 293–307.

20. Woodburn J., Coppola V., Stoner F. (2010). A description of filters for minimizing the time required for orbital conjunction computations. Advances in the Astronautical Sciences, 135:1157–1173.